Research in Astronomy and Astrophysics, 23:115015 (11pp), 2023 November https://doi.org/10.1088/1674-4527/acf6b2

Prediction of Short Stellar Activity Cycles using Derived and Established Empirical Relations between Activity and Rotation Periods

A. K. Althukair[1,2] and D. Tsiklauri[1]
[1] Department of Physics and Astronomy, School of Physical and Chemical Sciences, Queen Mary University of London, Mile End Road, London, E1 4NS, UK; a.k.althukair@qmul.ac.uk, d.tsiklauri@qmul.ac.uk
[2] Physics Department, College of Sciences, Princess Nourah Bint Abdulrahman University, Riyadh, P.O. Box 84428, Saudi Arabia
Received 2023 July 5; revised 2023 August 18; accepted 2023 September 1; published 2023 October 9

Abstract

In our previous work, we investigated the occurrence rate of super-flares on various types of stars and their statistical properties, with a particular focus on G-type dwarfs, using entire Kepler data. The said study also considered how the statistics change with stellar rotation period, which in turn, had to be determined. Using such new data, as a by-product, we found 138 Kepler IDs of F- and G-type main sequence stars with rotation periods less than a day ($P_{\rm rot} < 1$ day). On one hand, previous studies have revealed short activity cycles in F-type and G-type stars and the question investigated was whether or not short-term activity cycles are a common phenomenon in these stars. On the other hand, extensive studies exist which establish an empirical connection between a star's activity cycle and rotation periods. In this study, we compile all available Kepler data with $P_{\rm rot} < 1$ day, and rely on an established empirical relation between $P_{\rm cyc}$ and $P_{\rm rot}$ with the aim to provide predictions for very short $5.09 \leqslant P_{\rm cyc} \leqslant 38.46$ day cases in a tabular form. We propose an observation to measure $P_{\rm cyc}$ using a monitoring program of stellar activity (e.g., activity-related chromospheric emission S-index) or a similar means for the Kepler IDs found in this study in order put the derived empirical relations between $P_{\rm cyc}$ and $P_{\rm rot}$ derived here to the test. We also propose an alternative method for measuring very short $P_{\rm cyc}$, using flare-detection algorithms applied to future space mission data.

Key words: stars: activity – stars: flare – stars: rotation – stars: solar-type – stars: statistics – Sun: flares

1. Introduction

The 11 yr cycle of solar activity, discovered by Schwabe in 1844 (Schwabe 1844), is a significant phenomenon in solar and stellar physics. The cycle is manifested by a periodic change in solar activity, including the appearance of sunspots and changes in the Sun's magnetic field on this timescale. Smoothed sunspot numbers have been widely regarded as a proxy for solar activity over the past four centuries (Shepherd et al. 2014). The idea of the sunspot number was first introduced by Waldmeier (1961) in the mid-20th century, and it has since become a standard measure for quantifying solar activity. These numbers reveal that there are almost regular cycles of about 11 yr, reflecting the Sun's magnetic activity.

During the course of a solar cycle, the Sun experiences alternating periods of strong and weak activity known as solar maximum and minimum (Hathaway et al. 2002; Shepherd et al. 2014; Reinhold et al. 2017). As the solar cycle progresses, the magnetic field becomes more complex and twisted. This results in the emergence of sunspots, which are dark areas on the surface of the Sun with intense magnetic fields, and which vary in size and can last from days to several months (Petrovay & van Driel-Gesztelyi 1997), decaying into bright areas called faculae formed by smaller magnetic concentrations (Reinhold et al. 2017). During the active phase of the solar cycle (solar maximum), the sunspot number increases, and their size becomes larger on the surface of the Sun. At the same time, bright faculae also become more prominent. As the cycle progresses, the number of sunspots decreases, the overall brightness of the Sun reduces and the Sun enters its least active phase of the solar cycle (solar minimum). These dark and bright features on the Sun's surface contribute to variability in the total solar irradiance (TSI) (Marchenko et al. 2022). Therefore, the TSI data can capture the combined effects of the evolving dark and bright features during the solar cycle (Domingo et al. 2009; Reinhold et al. 2017).

Cyclic activity has been observed in stars other than the Sun through long-term brightness changes associated with increased occurrence of active regions on their surfaces or in their lower stellar atmospheres (Reinhold et al. 2017). The Mount Wilson HK Project, which started in 1966 and lasted until the end of the 20th century, was the first to conduct a systematic search for activity cycles in main sequence stars (Wilson 1978; Baliunas et al. 1995; Mittag et al. 2019a). By examining chromospheric emission within the Ca II H&K spectral lines, the magnetic field associated with active regions on stellar surfaces is vital in conveying energy to the

chromosphere. This heightened influx of energy into the chromosphere results in amplified chromospheric emission, notably observable in the central regions of the Ca II H&K spectral lines, as indicated by Reinhold et al. (2017). The measure of the chromospheric emission strength is described by the Mount Wilson S-index (Vaughan et al. 1978) or by the quantity $R'_{\rm HK}$ (Brandenburg et al. 2017). Vaughan & Preston (1980) investigated the chromospheric activity levels in main sequence F-G-K-M stars by measuring the chromospheric Ca II H&K emission fluxes. They noted that these stars display varying degrees of chromospheric activity and observed a noticeable lack in the number of F-G stars displaying intermediate activity compared to both highly active and less active stars. They suggested that the absence of such stars could be attributed to a decline in chromospheric activity as the stars age. Noyes et al. (1984a) examined the relationship between chromospheric activity, specifically the $R'_{\rm HK}$ activity index, and the Rossby number ${\rm Ro} = P_{\rm rot}/\tau_{\rm c}$ for a sample of main sequence stars of spectral type F or later, where $P_{\rm rot}$ is the rotational period of the star and $\tau_{\rm c}$ is a theoretically derived convective turnover time. They found a strong correlation between the $R'_{\rm HK}$ activity index and the Rossby number. However, in contrast to the findings of Vaughan & Preston (1980), Noyes et al. (1984a) did not find any signs of the "Vaughan–Preston gap." Noyes et al. (1984b) investigated the empirical relation between rotation period $P_{\rm rot}$, spectral type and activity cycle period $P_{\rm cyc}$ for 13 slowly rotating main-sequence stars. They found that the cycle period is related to the rotation period by a power law: $P_{\rm cyc} \propto P_{\rm rot}^{1.25}$. This relationship can alternatively be expressed as $P_{\rm cyc} \approx {\rm Ro}^{1.25} \approx (P_{\rm rot}/\tau_{\rm c})^{1.25}$ (Brandenburg et al. 2017; Mittag et al. 2023). For stars of spectral type G0-K5, Baliunas et al. (1995) observed a pattern of variation in the rotation period and the measure of chromospheric activity (S-index). Their research revealed that the chromospheric activity levels were high in young stars with fast rotation periods. Chromospheric activity and rotation rates of stars in the intermediate age range were average. Alternatively, the chromospheric activity levels were low in old stars with slow rotation periods. This observation supports the existence of the Vaughan–Preston gap, indicating that chromospheric activity and rotation change over time as the stars age. The relation between rotation periods and activity cycles of a sample of stars was investigated by Baliunas et al. (1996), who discovered a correlation between the two variables. In particular, they observed that stars with slower rotation periods exhibit longer activity cycles, while stars with faster rotation periods tend to have shorter activity cycles. According to Oláh & Strassmeier (2002), the relation between rotation periods and cycle lengths is more evident for stars with shorter activity cycles. However, the association becomes less clear for longer cycle lengths when considering more recent findings on the time variability of solar cycles.

In order to provide a background of results in this field of research, we now discuss previous literature. Vida et al. (2013) investigated the behavior and activity cycles of four fast-rotating late-type stars with ($P_{\rm rot} \leqslant 0.5$ day), highlighting the presence of 1 yr cycles and the correlation between rotation rate and cycle length. Vida et al. (2014) used the short-term Fourier transform, a time-frequency analysis method, to examine the light curves of 39 fast-rotating late-type active stars with rotation periods of less than one day. Nine of the selected stars showed indications of activity cycles with periods between 300 and 900 days. These cycles were inferred based on the observed variations in the typical latitude of the starspots. These variations, along with the differential rotation of the stellar surface, result in changes in the observed rotation period during the activity cycle. This variation in the rotation period was attributed to the movement and evolution of starspots at different latitudes of the star.

Reinhold et al. (2017) used four years of Kepler data to determine the cyclic variations in the amplitude of the light curve and the rotation period of stars by analyzing a sample of active stars and calculating the rotation period and variability amplitude for each star in each Kepler quarter. Then they searched for periodic variations in these time series using Lomb–Scargle periodograms and employed a false alarm probability (FAP) criterion for selection. The study's findings indicate that amplitude periodicities, associated with underlying activity cycles, are detected in 3203 stars with cycle periods ranging from 0.5 to 6 yr and rotation periods ranging from 1 to 40 days. According to Brandenburg et al. (2017)'s analysis of new observations and previous data, the longer and shorter cycle periods closely match expectations based on the average activity levels and rotation periods, which indicate a connection between stellar activity and stellar rotation.

Baliunas et al. (1995) reported an activity cycle of 11.6 yr in the F-type star τ Boo (HD 120136). However, the authors assigned an FAP "poor" grade to this finding. Mittag et al. (2017b) detected an activity cycle with a duration of 122 days in their analysis of the S-index data of τ Boo. This short activity cycle period suggests that τ Boo may exhibit variations on a relatively short timescale. Mittag et al. (2019a) focused on exploring the presence of short-term activity cycles in F-type stars, specifically using S-index time series data obtained with the Telescopio Internacional de Guanajuato Robótico Espectroscópico (TIGRE) facility. They utilized the generalized Lomb–Scargle periodogram method to analyze the data and search for periodic variations with a maximum length of 2 yr. Their sample of F-type stars identified four stars that exhibited cyclic variations with periods of less than a year. However, compared to solar-type stars with well-developed cyclic activity, the amplitudes of these short-term cyclic variations in F-type stars were smaller. Based on their findings, Mittag et al. (2019a) concluded that the activity behavior among

F-type stars differs from that of the Sun and cooler main sequence stars.

By studying 44 main sequence stars with confirmed activity cycles and rotation periods, Mittag et al. (2023) examined the relation between the length of the activity cycle and the Rossby number (Ro). They used empirical turnover periods based on the $B-V$ color index to calculate Rossby numbers, from which they deduced an empirical relationship between the Rossby number and the cycle duration. The study reported linear behavior in the double-logarithmic relationship between the Rossby number and cycle period. In addition, the relative convection zone depth was found to be correlated with cycle length and convective turnover time.

Besides the 11 yr solar cycle, shorter cycles were discovered called Rieger cycles. The original Rieger cycles were first identified in the Sun by Rieger et al. (1984) with a specific periodicity of approximately 154 days for flare occurrences. The Rieger-type cycles (RTCs) encompass cycles with periods (PRTC) ranging from 109 to 276 days. These RTCs were observed in various phenomena beyond solar flares, such as solar magnetic field and sunspot indexes, indicating their widespread nature. The underlying nature of RTCs remains unclear. The RTCs become more pronounced during the solar activity maximum. There is a potential connection between RTCs and the modulation of the solar magnetic dynamo process, as discussed in Arkhypov & Khodachenko (2021) and references therein. Possible reasons encompass the role of inertial g- and r-waves, also known as Rossby waves, as modulators of the emergence of magnetic flux in the Sun. Arkhypov & Khodachenko (2021) analyze photometric data from 1726 main sequence stars with varying effective temperatures and rotation periods to study RTCs in other stars. Two types of RTCs are identified among the surveyed stars. The activity cycles with RTC periods ($P_{\rm RTC}$) are independent of the stellar rotation period and are suggested to be driven by Kelvin waves. The second type are activity cycles with $P_{\rm RTC}$ proportional to the stellar rotation period and are suggested to be driven by Rossby waves.

The Parker (1955) model of the $\alpha-\Omega$ dynamo introduced the concept of migratory dynamo waves, which play a crucial role in generating the observed solar cycle (Mittag et al. 2023). The α-effect, arising from the twisting of rising magnetic field tubes due to Coriolis forces, creates the poloidal magnetic field required for the next sunspot cycle. This effect is responsible for the reversal of magnetic polarities between successive cycles (Parker 1955; Mittag et al. 2023). On the other hand, the Ω-effect, resulting from the differential rotation of the star, generates a toroidal magnetic field by stretching the magnetic field lines in a longitudinal direction. The combination of the α-effect and the Ω-effect leads to the formation of migratory dynamo waves, where the toroidal field is periodically regenerated and transformed into the poloidal field through the action of the α-effect. These migratory dynamo waves propagate and interact within the star's convective zone, causing the cyclic variations in the magnetic field (Mittag et al. 2023).

Now we describe existing theoretical knowledge about the possible relation between the magnetic cycle period and the rotation period of a star. In this context, according to Noyes et al. (1984b), the magnetic cycle period for G and K dwarfs, with convective turnover times ($\tau_{\rm c}$) between 11 and 26 days, is found to be proportional to the rotation period as follows:

$$1/P_{\rm cyc} \propto (\tau_{\rm c}/P_{\rm rot})^n, \tag{1}$$

where n is 1.25.

Simple dynamo models were discussed for understanding stellar magnetic activity and their implications for magnetic cycle periods in stars. Stix (1981) derived an equation to determine the critical dynamo number $D_{\rm crit}$ given by

$$D_{\rm crit} \sim (\Omega\tau_c)^2 \times \left(\frac{R_\star}{l}\right)^3, \tag{2}$$

where $(\Omega\tau_c)^2$ is the inverse squared Rossby number and $R_\star/l$ is the relative depth of turbulence, suggesting that the occurrence of dynamo action is contingent upon the interplay between stellar rotation and stellar structure.

Parker (1955) provides a relation for the magnetic cycle frequency, $\omega_{\rm mag\_cyc}$, that involves the shear, H, and the α-effect. Stix (1976) presented an equivalent expression for the magnetic cycle frequency derived by Parker (1955), in terms of angular velocity gradient, Ω', given by

$$\omega_{\rm mag\_cyc} = |\alpha\Omega'|^{\frac{1}{2}}, \tag{3}$$

indicating a proportional relationship between the cycle frequency and rotation frequency. Based on the model's assumptions, Equation (3) can be written as

$$P_{\rm mag\_cyc} = 2P_{\rm cyc} \approx \sqrt{\frac{R_\star}{l}}P_{\rm rot}, \tag{4}$$

where l here is the length scale of turbulence and $R_\star$ is the stellar radius. This equation indicates the theoretical prediction of the relation between the star's activity cycle and its rotation period, which is Equation (6) in Mittag et al. (2023).

According to the simple theoretical arguments quoted by Mittag et al. (2023), the magnetic cycle period $P_{\rm mag\_cyc}$ is proportional to the rotation period $P_{\rm rot}$. However, there is a modifying factor, $l/R_\star$ the relative depth of turbulence, which depends on the stellar structure, which itself may depend on the effective temperature or $B-V$ color index of the star. This factor is expected to vary among different stars, especially those with different sizes, masses and ages. The smallness of the inverse relative depth of the turbulence ensures that the period of the magnetic activity cycle $P_{\rm mag\_cyc}$ is small. However, precisely what factors guarantee smallness of $R_\star/l$ in a particular star is poorly understood. That is why it is unclear why stars with very short activity cycles, studied in this

Table 1
List of Star IDs with their Parameters, used in Previous Studies

HD/KIC	$T_{\rm eff}$	$B-V$	$P_{\rm rot}$(days)	Reference	$P^{S}_{\rm cyc}$(yr)	Reference
Sun	5777	0.642	25.4 ± 1	1	11 ± 2	1
HD 3651	5211	0.85	44	1	13.8 ± 0.4	1
HD 4628	5120	0.89	38.5 ± 2.1	1	8.6 ± 0.1	1
HD 10476	5244	0.836	35.2 ± 1.6	1	9.6 ± 0.1	1
HD 10780	5321	0.804	22.14 ± 0.55	2	7.53 ± 0.16	2
HD 16160	5060	0.918	48 ± 4.7	1	13.2 ± 0.2	1
HD 16673	6183	0.524	5.7	3	0.847 ± 0.006	5
HD 17051	6045	0.561	8.5 ± 0.1	1	1.6	1
HD 22049	5140	0.881	11.1 ± 0.1	1	2.9 ± 0.1	1
HD 26965	5282	0.82	43	1	10.1 ± 0.1	1
HD 30495	5804	0.632	11.4 ± 0.2	1	1.7 ± 0.3	1
HD 32147	4801	1.049	48	1	11.1 ± 0.2	1
HD 43587	5876	0.61	22.6 ± 1.9	4	10.44 ± 3.03	4
HD 75332	6089	0.549	4.8	5	0.493 ± 0.003	5
HD 75732	5167	0.869	37.4 ± 0.5	6	10.9	13
HD 76151	5714	0.661	15	1	2.5 ± 0.1	1
HD 100180	6013	0.57	14	1	3.6 ± 0.1	1
HD 103095	5449	0.754	31	1	7.3 ± 0.1	1
HD 120136	6245	0.508	3.05 ± 0.01	7	0.333 ± 0.002	7
HD 128621	5098	0.9	36.2 ± 1.4	1	8.1 ± 0.2	1
HD 140538	5645	0.684	20.71 ± 0.32	8	3.88 ± 0.02	8
HD 146233	5741	0.652	22.7 ± 0.5	1	7.1	1
HD 149661	5265	0.827	21.1 ± 1.4	1	4 ± 0.1	1
HD 160346	4975	0.959	36.4 ± 1.2	1	7 ± 0.1	1
HD 165341 A	5188	0.86	19.9	1	5.1 ± 0.1	1
HD 166620	5151	0.876	42.4 ± 3.7	1	15.8 ± 0.3	1
HD 185144	5366	0.786	27.7 ± 0.77	2	6.66 ± 0.05	2
HD 190406	5910	0.6	13.9 ± 1.5	1	2.6 ± 0.1	1
HD 201091	4764	1.069	35.4 ± 9.2	1	7.3 ± 0.1	1
HD 219834 B	5055	0.92	43	1	10 ± 0.2	1
KIC 8006161	5234	0.84	29.8 ± 3.1	1	7.4 ± 1.2	1
KIC 10644253	5943	0.59	10.9 ± 0.9	1	1.5 ± 0.1	1
Sun	5777	0.642	25.4 ± 1	1	10.3	14
HD 3651	5211	0.85	44	1	11.7	14
HD 4628	5120	0.89	38.5 ± 2.1	1	9.9	14
HD 10476	5244	0.836	35.2 ± 1.6	1	9.2	14
HD 10780	5321	0.804	22.14 ± 0.55	2	5.6	14
HD 16160	5060	0.918	48 ± 4.7	1	12.4	14
HD 16673	6183	0.524	5.7	3	0.9	15
HD 17051	6045	0.561	8.5 ± 0.1	1	1.4	14
HD 22049	5140	0.881	11.1 ± 0.1	1	2.6	14
HD 26965	5282	0.82	43	1	11.5	15
HD 30495	5804	0.632	11.4 ± 0.2	1	1.6	14
HD 32147	4801	1.049	48	1	11.7	15
HD 43587	5876	0.61	22.6 ± 1.9	4	10.4	14
HD 75332	6089	0.549	4.8	5	0.5	15
HD 75732	5167	0.869	37.4 ± 0.5	6	9.7	14
HD 76151	5714	0.661	15	1	2.4	14
HD 100180	6013	0.57	14	1	3.4	14
HD 103095	5449	0.754	31	1	9.6	14
HD 120136	6245	0.508	3.05 ± 0.01	7	0.3	14
HD 128621	5098	0.9	36.2 ± 1.4	1	9.2	14
HD 140538	5645	0.684	20.71 ± 0.32	8	4.5	14
HD 146233	5741	0.652	22.7 ± 0.5	1	7.2	14
HD 149661	5265	0.827	21.1 ± 1.4	1	5.3	14
HD 160346	4975	0.959	36.4 ± 1.2	1	9	14
HD 165341 A	5188	0.86	19.9	1	4.9	14
HD 166620	5151	0.876	42.4 ± 3.7	1	11.1	14

Table 1
(Continued)

HD/KIC	$T_{\rm eff}$	$B-V$	$P_{\rm rot}$(days)	Reference	$P^{S}_{\rm cyc}$(yr)	Reference
HD 185144	5366	0.786	27.7 ± 0.77	2	7.3	14
HD 190406	5910	0.6	13.9 ± 1.5	1	2.6	14
HD 201091	4764	1.069	35.4 ± 9.2	1	8.3	14
HD 219834 B	5055	0.92	43	1	11	15
KIC 8006161	5234	0.84	29.8 ± 3.1	1	7.7	14
KIC 10644253	5943	0.59	10.9 ± 0.9	1	1.8	14
102712791		0.277	0.96 ± 0.03	9	0.09 ± 0.008	9
102720703		0.514	10.2 ± 0.6	9	1.781 ± 0.356	9
102721955		0.431	2.17 ± 0.06	9	0.512 ± 0.055	9
102723038		1.404	8.6 ± 0.5	9	0.575 ± 0.019	9
102726103		0.767	3.7 ± 0.1	9	0.759 ± 0.058	9
102738457		0.592	12.9 ± 0.6	9	0.655 ± 0.06	9
102749950		0.657	5.4 ± 0.2	9	1.118 ± 0.071	9
102750723		1.143	1.44 ± 0.02	9	0.29 ± 0.019	9
102754736		0.48	6.9 ± 0.3	9	0.321 ± 0.022	9
102758108		0.641	6.1 ± 0.2	9	1.682 ± 0.151	9
102770332		2.055	4.2 ± 0.1	9	1.162 ± 0.112	9
102770893		0.874	4.3 ± 0.2	9	1.17 ± 0.123	9
102777006		1.177	1.33 ± 0.02	9	0.277 ± 0.022	9
102778595		1.157	11.8 ± 0.7	9	0.551 ± 0.041	9
102780281		1.304	3 ± 0.1	9	0.301 ± 0.022	9
61 Cygni A (HD 201091)	4545	1.069	35.7 ± 1.9	10	7.2 ± 1.3	10
HD 100563			7.73	5	0.61	5
HD 114710	5970	0.58	12.3 ± 1.1	1	9.6 ± 0.3	1
HD 128620	5809	0.71	22.5 ± 5.9	1	19.2 ± 0.7	1
HD 16673	6183	0.524	7.4 ± 0.07	5	0.85	5
HD 201092	4040	1.37	37.8 ± 7.4	1	11.7 ± 0.4	1
HD 219834 A	5461	0.8	42	1	21	1
HD 49933			3.45	5	0.58	5
HD 78366	5915	0.63	9.7 ± 0.6	1	5.9 ± 0.1	1
HD 81809	5623	0.8	40.2 ± 3	1	8.2 ± 0.1	1
solar analog HD 30495	5826	0.632	11.36 ± 0.17	11	1.67 ± 0.35	11
solar analog HD 45184	5871	0.62	19.98 ± 0.02	12	5.14	12
τ Boo		0.48	3.5	5	0.33	5

Note. The table illustrates a list of star IDs with their corresponding $B-V$ values, effective temperatures $T_{\rm eff}$, rotation periods $P_{\rm rot}$ with reference numbers and short branch cycle periods $P^{S}_{\rm cyc}$ with reference numbers.

References. (1) Brandenburg et al. (2017), (2) Olspert et al. (2018), (3) Noyes et al. (1984b), (4) Ferreira et al. (2020), (5) Mittag et al. (2019a), (6) Mittag et al. (2017a), (7) Mittag et al. (2017b), (8) Mittag et al. (2019b), (9) Ferreira Lopes et al. (2015), (10) Boro Saikia et al. (2016), (11) Egeland et al. (2015), (12) Flores et al. (2016) , (13) Baum et al. (2022), (14) Mittag et al. (2023).

paper, exist. All we can surmise is that the above theoretical arguments suggest $P_{\rm mag\_cyc}$ should scale as $\propto\sqrt{R_\star/l}$.

Activity cycles, characterized by variations in magnetic activity over time, are essential for understanding the fundamental mechanisms that drive the magnetic fields of stars. A range of methodologies exist for the identification of activity cycles in stars. One such approach involves integrated flux measurements by continuously monitoring the total amount of energy emitted by a star, enabling the detection of variations in its magnetic activity (Kopp et al. 2016; Reinhold et al. 2020). Another approach is the analysis of chromospheric emission lines from the outer atmosphere of a star. Additionally, tracking of starspots by observing the movement and changes in starspots on a star's surface serves as an indicator for fluctuations in magnetic activity (Montet et al. 2017). Nevertheless, it is important to acknowledge that these techniques include limitations regarding photometric precision and the small sample size in spectroscopic observations (Scoggins et al. 2019). An alternative approach involves detecting flares. Flares are a frequently observed phenomenon resulting from magnetic activity and are easier to detect, even at significant distances from stars. Wide-field photometric surveys allow for simultaneous monitoring of stars, making it possible to survey them for flare activity (Scoggins et al. 2019). The Sun experiences variations in its flare rate by a factor of 10 between the solar maximum and minimum activity periods. Scoggins

et al. (2019) focused on fluctuations in the frequency of flares from stars detected by the Kepler mission. The study examined a sample of 347 flare stars, which were selected based on having measured Kepler rotation periods, with a minimum of 100 candidate flare events. Scoggins et al. (2019) aimed to identify coherent variations in flare activity among these stars by computing the fractional luminosity emitted in flares. One star, KIC 8507979, was identified as the best candidate for flare activity variation. This star has a rotation period of 1.2 days and emits an average of 0.82 flares per day with energies exceeding 10^{32} erg over the 18 Kepler quarters. The study observed a decline in flare activity from KIC 8507979 over time. Although the flare census derived from the Kepler light curve of this star did not provide definitive evidence for a stellar activity cycle, the observed variation of approximately 0.1 dex per year was consistent with cyclic behavior over ten years or more.

The motivation for the current work is as follows: In Paper I (Althukair & Tsiklauri 2023a), we looked for super-flares on different types of stars and focused on G-type dwarfs using the entire Kepler data to study various aspects of statistical properties of the occurrence rate of super-flares. In Paper II (Althukair & Tsiklauri 2023b), as a by-product, we found 13 peculiar Kepler IDs that are Sun-like, slowly rotating cases with rotation periods of 24.5–44 days, and yet can produce a super-flare and six G-type and four M-type Kepler IDs with exceptionally large amplitude super-flares. As noted previously, these detections defy our current understanding of stars and hence deserve a further investigation. In this Paper III, the last in this series, we use the same data set as in Althukair & Tsiklauri (2023a) in order to study the empirical connection between a star's activity cycle and rotation period for a sample of F and G main sequence stars with rotation periods of less than one day. Here our aim is to provide predictions for very short activity cycle cases in a tabular form and to investigate in the future whether these short activity cycles are a common phenomenon in these stars or not. Section 2 presents the method used in this work which includes a reproduction of the Mittag et al. (2023) fit, the data representation and fit and the target selection method. The main findings of the study are presented in Section 3, and Section 4 concludes this work with our main conclusions.

2. Methods

In our study, we adopt the terminology used by Brandenburg et al. (2017), Mittag et al. (2023) to categorize branches into two types: the "inactive" branch, referred to as the short-cycle branch $P^S_{\rm cyc}$, and the "active" branch, referred to as the long-cycle branch $P^L_{\rm cyc}$. These terms were introduced for the first time in Brandenburg et al. (2017). According to Mittag et al. (2023), this notation is more accurate and aligned with the actual characteristics of the branches. Therefore, they suggested that these terms should be used in future studies to refer to the two branches.

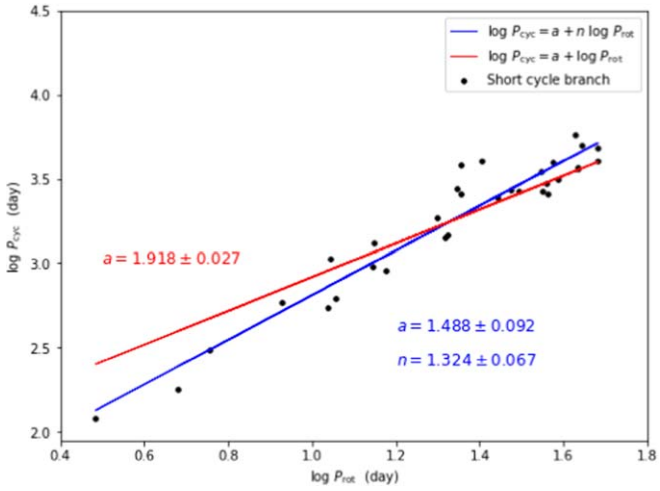

Figure 1. Log-scale of rotation period vs. log-scale of observed activity cycle period (short cycle branch) for a sample of stars taken from Mittag et al. (2023). The deduced fits of the $P_{\rm rot}$ vs. $P_{\rm cyc}$ relation are shown as solid lines. The blue line displays the fit when slope n is treated as an independent parameter while the red line delineates the fit with a fixed slope of $n = 1$.

2.1. Reproduction of Mittag et al. (2023) $P^S_{\rm cyc}$ versus P_{rot} Fit

In this subsection, we reproduce the fit between $P^S_{\rm cyc}$ and $P_{\rm rot}$ data from Mittag et al. (2023) to derive the fit parameters. First, we collected the data in Table 1, the first 32 rows are the observed activity cycle on the short-cycle branch $P^S_{\rm cyc}$ from Mittag et al. (2023), Table 1, along with the 32 corresponding rotation periods $P_{\rm rot}$. These cycle lengths and rotation periods can be found in Table 1. Then we plotted, in logarithmic scale, the rotation periods on the x-axis versus the observed cycle period on the y-axis as shown in Figure 1, using the empirical relation in Mittag et al. (2023) between the cycle periods and rotation periods in logarithmic terms that is given by

$$\log P_{\rm cyc} \approx a + n \log P_{\rm rot}. \quad (5)$$

Since the theoretical relation, Equation (4), implies a linear connection between $P_{\rm cyc}$ and $P_{\rm rot}$, we fitted the data using a Python *least-squares* fit, a common technique for determining the best-fitting parameters for a given model, for two different slope adjustments as in Mittag et al. (2023). Also, we computed the R^2 *coefficient of determination* to measure how well the model fits the data. An R^2 value of 1 means that the predictions from the regression fit the data perfectly. First, we set the slope n to be 1 and deduced the value of a parameter as $a = 1.918 \pm 0.027$ and the value of $R^2 = 0.87$. The red line in Figure 1 illustrates this trend. Then we repeated the fit by treating slope n as an independent variable to derive a and n

values as Equation (5) now becomes

$$\log P_{\rm cyc} \approx (1.488 \pm 0.092) + (1.324 \pm 0.067)\log P_{\rm rot}, \quad (6)$$

and the value of $R^2 = 0.93$. The fit given by Equation (6) is identical to that of Mittag et al. 2023. The blue line in Figure 1 represents this fit. It is obvious that the $n = 1$ relation does not fit the short period data, as Mittag et al. (2023) pointed out.

2.2. Data Representation and Fit

In this subsection, we repeat the fit between $P_{\rm rot}$ and $P^S_{\rm cyc}$ using a larger data sample, taken from Mittag et al. (2023) and other previous studies.

This sample, shown in Table 1, contains 92 $P_{\rm rot}$ and their 92 corresponding $P^S_{\rm cyc}$. In addition to the 32 observed activity cycles in Mittag et al. (2023), we aggregated 32 activity cycles on the short-cycle branch $P^S_{\rm cyc}$ computed by Mittag et al. (2023) together with the corresponding 32 rotation periods $P_{\rm rot}$. Furthermore, we included 28 activity cycles and their corresponding rotation periods that were collected from various other studies. These $P^S_{\rm cyc}$ were taken from Ferreira Lopes et al. (2015), Egeland et al. (2015), Boro Saikia et al. (2016), Flores et al. (2016), Brandenburg et al. (2017), Mittag et al. (2019a). The star ID, effective temperature ($T_{\rm eff}$), color index ($B - V$), $P_{\rm rot}$ and $P_{\rm cyc}$ are shown in Table 1. Unavailable data are left blank in the table. It should be noted that we used in the fit two $P^S_{\rm cyc}$ values for each of the 32 star IDs in Mittag et al. (2023), one was the observed $P^S_{\rm cyc}$ by a previous study, and the other was the calculated $P^S_{\rm cyc}$ by Mittag et al. (2023), except for HD 16673 for which we collected three $P^S_{\rm cyc}$ due to the multiple sources, as shown in Table 1. References for each $P_{\rm rot}$ and $P^S_{\rm cyc}$ are shown in Table 1.

In the same way as in Section 2.1, we utilized the empirical relation between $P_{\rm rot}$ and $P_{\rm cyc}$ in logarithmic scale given by Equation (5) using the new data set in Table 1 to produce the fit parameters a and n. We performed a *least-squares* fit in Python to fit the data using two different slope adjustments again, one with a fixed slope n of 1 and another with the n treated as a free variable. This fit is depicted in Figure 2. For the fit with a fixed slope of 1, we determined the value for the parameter $a = 1.890 \pm 0.024$ and $R^2 = 0.83$. This trend is visualized by the red line in Figure 2. While for the fit with the slope n treated as a free variable, we deduced values for the parameters a and n as $a = 1.585 \pm 0.064$, $n = 1.256 \pm 0.051$ and $R^2 = 0.87$. This fit is represented by the blue line in Figure 2, so that Equation (5) now becomes

$$\log P_{\rm cyc} \approx (1.585 \pm 0.064) + (1.256 \pm 0.051)\log P_{\rm rot}. \quad (7)$$

We note that our value of $n = 1.256 \pm 0.051$ with the extended data set is closer to Noyes et al. (1984b)'s $n = 1.25$ than Mittag et al. (2023)'s $n = 1.324 \pm 0.067$.

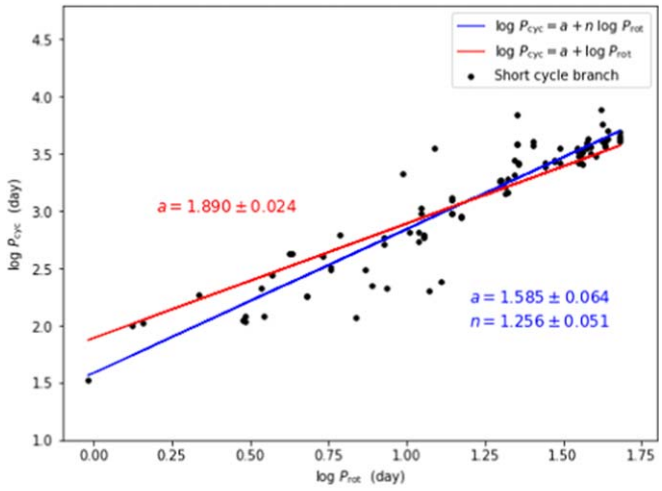

Figure 2. Log-scale of rotation period vs. log-scale of cycle period (short cycle branch) for a sample of 92 stars taken from previous studies in Table 1. The deduced fit of the $P_{\rm rot}$ vs. $P_{\rm cyc}$ relation is displayed as solid lines. The blue line indicates the fit where slope n is treated as an independent parameter while the red line shows the fit with a fixed slope of $n = 1$.

2.3. Data Samples

One of the main challenges in studying the relation between cycle length and rotation period is the lack of well-known and accurately measured activity cycles. This limitation introduces uncertainties in the derived empirical relations (Mittag et al. 2023). To overcome these challenges, it is crucial to obtain more reliable cycle periods, particularly for long-period cycles. Achieving this requires long-term time series observations of stars to gather comprehensive and accurate data on their activity cycles (Mittag et al. 2023). Therefore, when looking for activity cycles, it is more efficient to monitor fast-rotating objects, as cycles can be discovered within a few years of observation, as opposed to stars with longer rotation periods (Vida et al. 2013). For this reason, we chose our sample for this study to include fast-rotating main sequence stars of type F and G from Kepler data with well-known rotation periods of less than one day. First, we collected all Kepler IDs which have well-known rotation periods. We then selected targets with rotation periods of less than a day. Using Gaia Data Release 2 (Gaia DR2), we identified F- and G-type main sequence stars by their effective temperatures and radii based on the Harvard Spectral classification. The ranges of the effective temperature are 6000–7500 K and 5200–6000 K for F- and G-types, respectively. We thus obtained a total of 811 Kepler IDs of F- and G-type stars with less than one day rotation period. By applying the radius restriction of 1.15–1.4 $R_\odot$ and 0.96–1.15 $R_\odot$ to main sequence stars for F- and G-types, respectively, the final data sample reduced to 138 Kepler targets with a number of 83 F-type and 55 G-type main

Table 2
Lists of the 138 Kepler IDs with their Parameters and Predicted P_{cyc}

KIC	T_{eff}	$R_{\odot}$	P_{rot}(days)	Reference	P_{cyc}(days)	KIC	T_{eff}	$R_{\odot}$	P_{rot}(days)	Reference	P_{cyc}(days)
757099	5521	1.05	0.36	1	10.66	6877871	6508	1.40	0.54	2	17.74
1028018	5544	1.14	0.62	2	21.10	6948098	6095	1.29	0.57	3	18.98
1721795	6534	1.31	0.89	2	33.22	6961285	5802	0.98	0.45	2	14.11
1872192	5316	0.98	0.67	2	23.26	6962901	5601	0.97	0.98	2	37.50
2557335	5568	1.01	0.24	2	6.41	7199002	6381	1.24	0.57	2	18.98
2558273	6673	1.35	0.99	2	37.98	7199013	5286	0.96	0.57	2	18.98
2715228	6374	1.30	0.99	1	37.98	7199037	6024	1.36	0.57	2	18.98
2715410	5997	1.11	0.90	1	33.69	7354297	5481	1.05	0.95	2	36.06
2849645	5424	1.06	1.00	2	38.46	7461022	6168	1.28	0.59	2	19.82
2985825	6783	1.23	0.94	3	35.58	7678509	6644	1.22	0.96	2	36.54
3124412	6302	1.21	0.93	1	35.11	7707736	5644	1.09	0.76	2	27.25
3241517	6283	1.34	0.78	3	28.15	7816211	6050	1.32	0.29	2	8.12
3352959	6476	1.37	0.76	2	27.25	7909399	6574	1.40	0.82	2	29.97
3356577	6746	1.39	0.63	4	21.53	7915824	6231	1.39	0.74	2	26.35
3448722	5872	1.13	0.41	2	12.55	7973882	5512	1.06	0.35	2	10.29
3448817	6792	1.33	0.95	4	36.06	8016369	6734	1.34	0.77	1	27.70
3459311	5789	1.05	0.98	2	37.50	8043256	6680	1.27	0.93	2	35.11
3550386	6006	1.30	0.32	2	9.19	8144578	6639	1.32	0.59	2	19.82
3836772	6210	1.32	0.69	2	24.13	8197275	5604	1.14	0.44	2	13.71
3869099	5607	1.01	0.29	2	8.12	8264155	6738	1.33	0.91	4	34.16
4175618	5369	1.05	0.41	2	12.55	8264659	5417	1.12	0.97	1	37.02
4283120	6202	1.25	0.52	2	16.92	8285970	5639	1.14	0.57	2	18.98
4374659	5824	1.03	0.23	2	6.07	8313378	6624	1.31	0.54	2	17.74
4386947	5681	1.14	0.65	2	22.39	8382253	5695	1.01	0.63	3	21.53
4464528	6392	1.38	0.22	2	5.74	8393626	5893	1.15	0.43	2	13.32
4464530	6545	1.30	0.22	2	5.74	8420730	5770	1.08	0.25	2	6.74
4570231	5661	0.99	0.54	1	17.74	8651921	6473	1.29	0.95	2	36.06
4660562	5677	0.96	0.77	1	27.70	8687209	5650	1.00	0.77	1	27.70
4762130	6202	1.35	0.80	2	29.06	8804962	6586	1.23	0.90	2	33.69
4774370	6546	1.36	0.93	2	35.11	8892124	5263	1.01	0.72	2	25.46
4816098	6239	1.29	0.95	1	36.06	8916436	6566	1.35	0.87	1	32.29
4850965	5503	1.04	0.61	2	20.67	9146690	5387	1.11	0.72	2	25.46
4949214	6511	1.36	0.92	2	34.64	9206726	6876	1.31	0.46	4	14.50
4949350	6587	1.40	0.88	2	32.75	9306290	5571	1.04	0.82	2	29.97
4949766	6587	1.39	0.81	2	29.52	9393015	5877	1.01	0.24	2	6.41
5038288	5785	0.99	0.88	2	32.75	9456932	5875	0.97	0.53	2	17.33
5107198	6077	1.36	0.36	2	10.66	9474101	5945	1.10	0.21	2	5.42
5273178	6774	1.32	0.88	2	32.75	9594038	6694	1.31	0.94	4	35.58
5397765	6251	1.34	0.94	2	35.58	9640204	6620	1.33	0.53	2	17.33
5426665	6323	1.38	0.39	2	11.79	9640472	6076	1.34	0.34	2	9.92
5444276	6475	1.31	0.71	2	25.01	9710612	5867	1.08	0.39	2	11.79
5450307	6398	1.24	0.99	3	37.98	9730249	6479	1.34	0.91	2	34.16
5480545	6535	1.31	0.93	2	35.11	9896552	6279	1.26	0.87	1	32.29
5514866	5487	0.97	0.28	2	7.77	9897710	5840	1.08	0.43	2	13.32
5514871	5220	1.06	0.28	2	7.77	9965888	5589	1.13	0.31	2	8.83
5543840	6518	1.20	0.82	2	29.97	9970838	6429	1.25	0.96	2	36.54
5623538	6729	1.32	0.99	1	37.98	10023062	6469	1.38	0.89	2	33.22
5623852	5886	1.10	0.57	2	18.98	10134084	5926	1.00	0.55	5	18.15
5629449	6897	1.31	0.71	1	25.01	10490282	5504	1.05	0.79	2	28.60
5646176	6302	1.20	0.99	1	37.98	10614890	5283	1.06	1.00	2	38.46
5795235	6517	1.36	0.91	2	34.16	10809099	6051	1.31	0.91	2	34.16
5898014	6697	1.35	0.83	2	30.43	11017401	5648	1.09	0.80	2	29.06
5988566	6299	1.20	0.44	2	13.71	11018874	6454	1.30	0.99	2	37.98
6114118	6234	1.24	0.94	2	35.58	11247377	6184	1.38	0.40	2	12.17
6114140	6384	1.16	0.93	3	35.11	11349677	6076	1.23	0.84	1	30.90
6145032	6315	1.28	0.81	1	29.52	11400413	6781	1.34	0.76	4	27.25
6149358	6660	1.28	0.89	2	33.22	11498689	5464	1.10	0.31	2	8.83
6219870	5663	1.05	0.81	1	29.52	11653059	6160	1.26	0.29	2	8.12
6224148	6230	1.18	0.20	2	5.09	11924842	5494	1.13	0.84	5	30.90

Table 2
(Continued)

KIC	$T_{\rm eff}$	$R_{\odot}$	$P_{\rm rot}$(days)	Reference	$P_{\rm cyc}$(days)	KIC	$T_{\rm eff}$	$R_{\odot}$	$P_{\rm rot}$(days)	Reference	$P_{\rm cyc}$(days)
6385867	5306	1.06	0.58	1	19.40	11969131	6444	1.23	0.63	1	21.53
6386598	6658	1.37	0.76	2	27.25	12067121	6211	1.33	0.43	5	13.32
6391602	5782	0.99	0.42	2	12.94	12108612	5695	1.09	0.71	2	25.01
6421219	6191	1.36	0.79	2	28.60	12119534	5296	0.98	0.64	2	21.96
6449077	6366	1.31	0.94	2	35.58	12121738	6134	1.31	0.73	2	25.90
6529902	6604	1.38	0.29	2	8.12	12157161	6513	1.26	0.78	2	28.15
6693864	6846	1.35	0.86	1	31.82	12157799	6117	1.17	0.89	5	33.22
6836589	5628	1.15	0.73	2	25.90	12354328	5251	0.97	0.81	2	29.52
6846595	6718	1.26	0.99	1	37.98	12356839	5605	1.14	0.35	2	10.29
6854461	6547	1.39	0.95	3	36.06	12418959	6427	1.36	0.78	2	28.15

Note. Effective temperature $T_{\rm eff}$ and radius $R_{\odot}$ was taken from Gaia DR2.
References. (1) Santos et al. (2021), (2) McQuillan et al. (2014), (3) Reinhold & Gizon (2015), (4) Chowdhury et al. (2018), (5) Yang & Liu (2019).

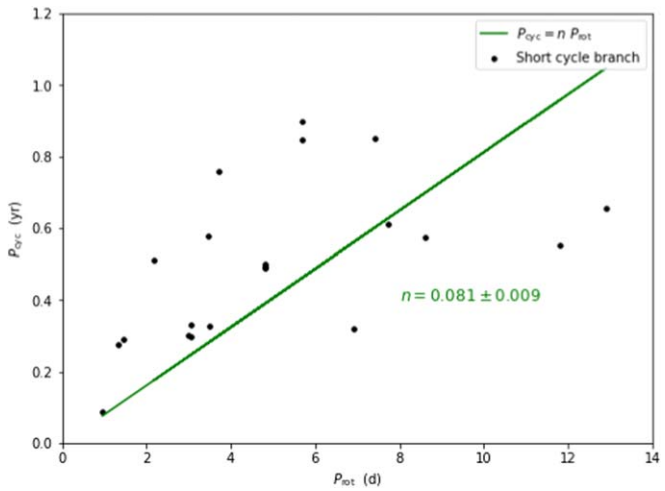

Figure 3. $P_{\rm rot}$ vs. $P_{\rm cyc}$ using a simple linear regression without an intercept for a sample of stars whose $P_{\rm cyc}$ is less than 1 year. The determined fit of the $P_{\rm rot}$ vs. $P_{\rm cyc}$ relation is shown as a solid green line.

sequence stars; 71.74% of the rotation periods for these stars were taken from McQuillan et al. (2014), 15.94% from Santos et al. (2021), 5.07% from Reinhold & Gizon (2015), 4.35% from Chowdhury et al. (2018) and 2.90% from Yang & Liu (2019). These 138 Kepler targets are listed in Table 2 with their effective temperature, radius, rotation period and the references for these rotation periods.

3. Results

Using a data set of 138 Kepler IDs with $P_{\rm rot}$ ranging from 0.202 to 0.997 day, we provide a prediction for the corresponding value of their $P_{\rm cyc}^{S}$, by applying the empirical relation between $P_{\rm cyc}$ and $P_{\rm rot}$ with the derived parameters in Equation (7). Hence we obtained the predicted values of $P_{\rm cyc}$ from

$$P_{\rm cyc} \approx 10^{(1.585\pm0.064)+(1.256\pm0.051)\log P_{\rm rot}}. \quad (8)$$

From Equation (8), we calculated 138 $P_{\rm cyc}$ for 83 F-type and 55 G-type main sequence stars whose rotation period is less than a day. The shortest $P_{\rm cyc}$ is equal to 5.09 days while the longest $P_{\rm cyc}$ is equal to 38.46 days. All the 138 predicted $P_{\rm cyc}$ are listed in Table 2.

After predicting the values of the activity cycles for our extended, compared to Mittag et al. (2023), data sample, we wish to examine the theoretical prediction given by Equation (4) on short $P_{\rm cyc} < 1$ yr. This is because the latter equation is a theoretical prediction, based on first physical principles, as opposed to an empirical fit, which lacks any theoretical or conceptual justification. Therefore, we focus on the activity cycles derived from previous studies, as presented in Table 1. We choose 20 stars whose $P_{\rm cyc}$ is less than a year and plot the fit between $P_{\rm rot}$ and $P_{\rm cyc}$ as depicted in Figure 3 using a simple linear regression without an intercept given by

$$P_{\rm cyc}\ [\rm yr] = n\ P_{\rm rot}\ [\rm days]. \quad (9)$$

We obtained the slope $n = 0.081 \pm 0.009$ and the R^2 value is 0.997. Although the R^2 value for the fit is near unity, there is a large scatter indicating a poor quality fit. Note that $P_{\rm cyc}$ here is in years, as in Figure 14 from Mittag et al. (2019a). Therefore, for the lower and upper bounds of our 138 Kepler IDs with $P_{\rm rot}$ ranging from 0.202 day to 0.997 day, this simple theoretically justified equation predicts $P_{\rm cyc} = 0.081 \times 0.202 \times 365.25 = 5.98$ days and $0.081 \times 0.997 \times 365.25 = 29.50$ days, which are not very different from applying the more accurate power law fit using Equation (8) of 5.09 days and 38.46 days, respectively.

4. Conclusions

In this work, we studied the empirical relation between star activity cycle and rotation period. First, we reproduced the fit

between $P_{\rm rot}$ and $P_{\rm cyc}$ using Mittag et al. (2023) data and obtained the following fit parameters $\log P_{\rm cyc} \approx (1.488 \pm 0.092) + (1.324 \pm 0.067)\log P_{\rm rot}$, which are the same parameters as in Mittag et al. (2023). Then, using a larger data set made up of $P_{\rm rot}$ and their associated $P_{\rm cyc}$ taken from prior studies, we again re-examined the fit between $P_{\rm rot}$ and $P_{\rm cyc}$ and obtained the following fit parameters $\log P_{\rm cyc} \approx (1.585 \pm 0.064) + (1.256 \pm 0.051)\log P_{\rm rot}$. Using these new parameters, we applied this relation to a sample of 83 F-type and 55 G-type main sequence stars with rotation periods of less than one day. The objective was to predict short activity cycles for these stars, aiming to ascertain, in future studies, if short activity cycles are a common occurrence in these stars or not. As a result, we derived 138 predicted $P_{\rm cyc}$ ranging from 5.09 to 38.46 days, which are listed in Table 2.

The usefulness of measuring short stellar activity cycles hinges on two main general difficulties:

(i) If the monitoring program of stellar activity (e.g., activity-related chromospheric emission S-index or similar) is used as in references such as Mittag et al. (2019a); or Baum et al. (2022), then cadence time of observations is too long, e.g., according to Table 2 from the latter reference cadence could be 87 observations per year, i.e., $365/87 = 4$ days. Resolving activity cycles with $5.09 \leqslant P_{\rm cyc} \leqslant 38.46$ days with such cadence would be nearly impossible.

(ii) If Kepler data light curves are used for, e.g., plotting number of flares per day versus time then a large number of flare detections would be necessary to have reliable statistics. However, the problem is long cadence, 30 minutes, for the mainstream Kepler data. The photometer used by Kepler is sensitive to wavelengths ranging from 400 to 865 nm, covering the entire visible spectrum and a fraction of the infrared. The accuracy of the photometer on Kepler is approximately 0.01% or 0.1 mmag, when 30 minute integration times are used while considering stars with a magnitude of 12. Kepler's 30 minute integration detected flare amplitudes are less than 0.1% of the stellar value and have energies of 2×10^{33} erg. The duration of the flares ranged from one to three hours, with a rapid increase followed by a slow, exponential decline (Maehara et al. 2012). When Kepler data are taken at a higher cadence or sampling rate of one minute, the accuracy of the measurements decreases. However, this higher cadence enables Kepler to detect flares that are too brief to be detected reliably using the main 30 minute integrations. With the one-minute cadence, Kepler can detect flares with energies as low as 10^{32} erg (Maehara et al. 2015).

It is worth noting that earlier studies exist using different observations where the energy involved in the observed transient brightening is estimated to range from 10^{25} to 10^{29} erg (Shimizu 1995). Also, as far as the Sun is concerned, studies exist (Mason et al. 2023) which consider flare frequency as a function of flare energy in the range 10^{27}–10^{31} erg, but this is only applicable to the Sun.

In order to have good statistics for the Kepler IDs considered, we need to detect flares with energies 10^{27-32} erg in order to see a variation in the number of flares per day on a timescale of $5.09 \leqslant P_{\rm cyc} \leqslant 38.46$ days. To achieve this goal, a new space mission is necessary with short time cadence (<1 minute) and photometric accuracy <0.01%.

A typical example of such a proposed hypothetical space mission would record data on the number of flares per day for each target. These data can be presented in bins of, e.g., one-day width where the bin heights would show the number of flares detected in that bin. These bins would then exhibit a periodic variation over time. Fitting a sinusoidal curve then would enable deducing the activity cycle period. Thus, through this periodic variation, we could potentially detect the target's magnetic activity cycle period. In some sense, our approach is similar to that of Scoggins et al. (2019). However, their observation was so short in duration that only decrease in the flare activity was seen. A longer duration of observations from a proposed new space mission would enable seeing periodic variation and hence deducing the activity cycle period.

An alternative option could be conducting a shorter cadence ground-based S-index monitoring program of stellar activity with cadence ≈1 day or less. However it is unclear whether this is technically feasible. In any case, the present study provides predictions for $5.09 \leqslant P_{\rm cyc} \leqslant 38.46$ days and we hope that either future space or ground-based observational missions will put our predictions to the test. Until such time, the jury is still out.

Acknowledgments

Some of the data presented in this paper were obtained from the Mikulski Archive for Space Telescopes (MAST). STScI is operated by the Association of Universities for Research in Astronomy, Inc., under NASA contract NAS5-26555. Support for MAST for non-HST data is provided by the NASA Office of Space Science via grant NNX13AC07G and by other grants and contracts.

The authors would like to thank Deborah Kenny of STScI for kind assistance in obtaining the data, and Cozmin Timis and Alex Owen of Queen Mary University of London for their assistance in data handling at the Astronomy Unit.

A. K. Althukair wishes to thank Princess Nourah Bint Abdulrahman University, Riyadh, Saudi Arabia and Royal Embassy of Saudi Arabia Cultural Bureau in London, UK for the financial support of her PhD scholarship, held at Queen Mary University of London.

Authors would like to thank an anonymous referee whose comments greatly improved this manuscript.

Data Availability

Some of the data underlying this article were accessed from the Mikulski Archive for Space Telescopes (MAST) https://mast.stsci.edu/portal/Mashup/Clients/Mast/Portal.html. This paper also has made use of data from the European Space Agency (ESA) mission Gaia (https://www.cosmos.esa.int/gaia), processed by the Gaia Data Processing and Analysis Consortium (DPAC, https://www.cosmos.esa.int/web/gaia/dpac/consortium). Funding for the DPAC has been provided by national institutions, in particular the institutions participating in the Gaia Multilateral Agreement. The derived data generated in this research will be shared on reasonable request to the corresponding author.

ORCID iDs

A. K. Althukair https://orcid.org/0000-0003-4075-4440
D. Tsiklauri https://orcid.org/0000-0001-9180-4773

References

Althukair, A. K., & Tsiklauri, D. 2023a, RAA, 23, 085017
Althukair, A. K., & Tsiklauri, D. 2023b, RAA, 23, 105010
Arkhypov, O. V., & Khodachenko, M. L. 2021, A&A, 651, A28
Baliunas, S. L., Donahue, R. A., Soon, W. H., et al. 1995, ApJ, 438, 269
Baliunas, S. L., Nesme-Ribes, E., Sokoloff, D., & Soon, W. H. 1996, ApJ, 460, 848
Baum, A. C., Wright, J. T., Luhn, J. K., & Isaacson, H. 2022, AJ, 163, 183
Boro Saikia, S., Jeffers, S. V., Morin, J., et al. 2016, A&A, 594, A29
Brandenburg, A., Mathur, S., & Metcalfe, T. S. 2017, ApJ, 845, 79
Chowdhury, S., Joshi, S., Engelbrecht, C. A., et al. 2018, Ap&SS, 363, 260
Domingo, V., Ermolli, I., Fox, P., et al. 2009, SSRv, 145, 337
Egeland, R., Metcalfe, T. S., Hall, J. C., & Henry, G. W. 2015, ApJ, 812, 12
Ferreira Lopes, C. E., Leão, I. C., de Freitas, D. B., et al. 2015, A&A, 583, A134
Ferreira, R. R., Barbosa, R., Castro, M., et al. 2020, A&A, 640, A46
Flores, M., González, J. F., Jaque Arancibia, M., Buccino, A., & Saffe, C. 2016, A&A, 589, A135
Hathaway, D. H., Wilson, R. M., & Reichmann, E. J. 2002, SoPh, 211, 357
Kopp, G., Krivova, N., Wu, C. J., & Lean, J. 2016, SoPh, 291, 2951
Maehara, H., Shibayama, T., Notsu, S., et al. 2012, Natur, 485, 478
Maehara, H., Shibayama, T., Notsu, Y., et al. 2015, EP&S, 67, 59
Marchenko, S. V., Lean, J. L., & DeLand, M. T. 2022, ApJ, 936, 158
Mason, J. P., Werth, A., West, C. G., et al. 2023, ApJ, 948, 71
McQuillan, A., Mazeh, T., & Aigrain, S. 2014, ApJS, 211, 24
Mittag, M., Hempelmann, A., Schmitt, J. H. M. M., et al. 2017a, A&A, 607, A87
Mittag, M., Robrade, J., Schmitt, J. H. M. M., et al. 2017b, A&A, 600, A119
Mittag, M., Schmitt, J. H. M. M., Hempelmann, A., & Schröder, K. P. 2019a, A&A, 621, A136
Mittag, M., Schmitt, J. H. M. M., Metcalfe, T. S., Hempelmann, A., & Schröder, K. P. 2019b, A&A, 628, A107
Mittag, M., Schmitt, J. H. M. M., & Schröder, K. P. 2023, arXiv:2306.05866
Montet, B. T., Tovar, G., & Foreman-Mackey, D. 2017, ApJ, 851, 116
Noyes, R. W., Hartmann, L. W., Baliunas, S. L., Duncan, D. K., & Vaughan, A. H. 1984a, ApJ, 279, 763
Noyes, R. W., Weiss, N. O., & Vaughan, A. H. 1984b, ApJ, 287, 769
Oláh, K., & Strassmeier, K. G. 2002, AN, 323, 361
Olspert, N., Lehtinen, J. J., Käpylä, M. J., Pelt, J., & Grigorievskiy, A. 2018, A&A, 619, A6
Parker, E. N. 1955, ApJ, 122, 293
Petrovay, K., & van Driel-Gesztelyi, L. 1997, SoPh, 176, 249
Reinhold, T., Cameron, R. H., & Gizon, L. 2017, A&A, 603, A52
Reinhold, T., & Gizon, L. 2015, A&A, 583, A65
Reinhold, T., Shapiro, A. I., Solanki, S. K., et al. 2020, Sci, 368, 518
Rieger, E., Share, G. H., Forrest, D. J., et al. 1984, Natur, 312, 623
Santos, A. R. G., Breton, S. N., Mathur, S., & García, R. A. 2021, ApJS, 255, 17
Schwabe, H. 1844, AN, 21, 233
Scoggins, M. T., Davenport, J. R. A., & Covey, K. R. 2019, RNAAS, 3, 137
Shepherd, S. J., Zharkov, S. I., & Zharkova, V. V. 2014, ApJ, 795, 46
Shimizu, T. 1995, PASJ, 47, 251
Stix, M. 1976, in Basic Mechanisms of Solar Activity, Vol. 71 ed. V. Bumba & J. Kleczek, 367
Stix, M. 1981, SoPh, 74, 79
Vaughan, A. H., & Preston, G. W. 1980, PASP, 92, 385
Vaughan, A. H., Preston, G. W., & Wilson, O. C. 1978, PASP, 90, 267
Vida, K., Kriskovics, L., & Oláh, K. 2013, AN, 334, 972
Vida, K., Oláh, K., & Szabó, R. 2014, MNRAS, 441, 2744
Waldmeier, M. 1961, The Sunspot-activity in the Years 1610–1960 (Zurich: Schulthess)
Wilson, O. C. 1978, ApJ, 226, 379
Yang, H., & Liu, J. 2019, ApJS, 241, 29